Supplementary Information

Waste–to–Waste Valorization: Sustainable Palladium Recovery from Real Spent Catalytic Converter Leachates Using Chicken Feathers

Amir Nobahar [1], Flavia N. Braga[1,2], Filipe H. B. Sosa[1], Nicolas Schaeffer[1], João A.P. Coutinho[1], Helena Passos[2*]

[1]CICECO – Aveiro Institute of Materials, Department of Chemistry, University of Aveiro, 3810–193 Aveiro, Portugal

[2]LSRE–LCM, ALiCE, Faculty of Engineering, University of Porto, Rua Dr. Roberto Frias, 4200–465 Porto, Portugal

*Corresponding author: hpassos@fe.up.pt

1. Experimental

1.1. Materials

Standard metal solutions of 1000 $mg.L^{-1}$ were purchased for Pt in 0.5 M HCl (BDH Chemicals Ltd, Poole, England) and Rh in 5% HCl (Sigma–Aldrich, Switzerland). Stock solutions of 1000 $mg.L^{-1}$ of Pd, Fe, Zn and Ce, were prepared by dissolving proper quantities of analytical–grade reagents, including $PdCl_2$ (Sigma–Aldrich, USA), $FeCl_3$ (Thermo Fisher, Germany), $ZnCl_2$ (Thermo Scientific, USA), and $CeCl_3 \cdot 7H_2O$ (Merck, Germany), in deionized water.

Ethanol (96%) was purchased from Carlo Erba Reagents (RE–Pure), while thiourea (99% purity) was supplied by Acros Organics. Technical grade sodium hydroxide and sulfuric acid (95–97%) were obtained from VWR Chemicals. Hydrochloric acid (~37%, analytical reagent grade) was supplied by Fisher Scientific, and nitric acid (≥65%) along with the Yttrium standard (996 mg/L ± 4 mg/L in nitric acid, TraceCERT) were sourced from Sigma–Aldrich. Silicone solution (in isopropanol) was acquired from Serva Electrophoresis GmbH, and poly(vinyl alcohol) (87–90% hydrolyzed, average molecular weight: 30,000–70,000) was also provided by Sigma–Aldrich. Working solutions of lower concentrations were systematically prepared by diluting the main stock solutions as required.

Urea (≥99.5% purity) for analytical use was obtained from Acros Organics. Dithiothreitol (DTT) was purchased from NZYTech and stored dry at −20 °C. Iodoacetamide (BioUltra grade) was sourced from Sigma Life Science. All reagents were of analytical or molecular biology grade and used without further purification.

CFs were collected from Campoaves Company in Oliveira de Frades, Portugal.

Starting SACCs materials were provided by the Portuguese company VALORCAR (Sociedade de Gestão de Veículos em Fim de Vida, Lda., Aveiro, Portugal). Four end–of–life SACCs materials were obtained for this experimental work: (1) a SACC from a Volkswagen Golf III (1991–1999 production model) with a gasoline engine; (2) a Peugeot 106 (1991–2004 production model) with a gasoline engine; (3) a SACC from a Renault Clio II (1998–2002 production model) with a diesel engine; and (4) a diesel particulate filter (DPF) from a diesel engine in a silicon carbide (SiC) matrix.

1.2. Characterization of the adsorbent

The adsorbent before and after adsorption was characterized using a variety of analytical techniques. The particle size distribution of the ground CF was determined using a laser scattering analyzer (HORIBA LA–960, HORIBA Scientific, Japan) operating in Fraunhofer mode. Zeta–potential measurements were performed using a laser Doppler electrophoresis analyzer (Malvern Zetasizer). Suspended CF samples were measured at 25 °C in disposable cells following standard electrophoretic mobility protocols. Raman spectroscopy was performed using a FT–RAMAN

BRUKER MultiRAM spectrometer. The analysis utilized a Nd–YAG laser with a wavelength of 1064 nm and a power of 50 mW. The spectral resolution was set at 4 cm^{-1}, with 1000 scans collected over a range of 4000 to 50 cm^{-1}. Fourier Transform Infrared (FTIR) spectroscopy was conducted in the spectral range of 4000–400 cm^{-1} using a FTIR system spectrum BX, PerkinElmer, equipped with a single horizontal Golden Gate ATR cell and a diamond crystal.

The morphology and elemental composition of CFs before and after the sorption process were evaluated using scanning electron microscopy coupled with energy–dispersive spectroscopy (SEM–EDS) on a HITACHI SU–70 apparatus operating at 25 kV, following carbon sputter–coating. Scanning transmission electron microscopy (STEM) was performed on a Hitachi HD–2300 operated at 200 kV. Samples were dispersed in ethanol, sonicated for 5 min to break up agglomerates, and drop–cast onto carbon–coated copper grids. Imaging was conducted under slow–scan conditions (20 s per frame) with emission currents of 6–9 nA.

X–ray photoelectron spectroscopy (XPS) was conducted using a Thermo Scientific NEXSA system equipped with a monochromatized Al Kα X–ray source (photon energy: 1486.6 eV). Due to the non–conductive nature of the samples, surface charging was minimized using a dual neutralization system: a low–energy electron flood gun (0–14 eV) and a low–energy argon ion source. Measurements were performed at a photoelectron take–off angle of 90° relative to the sample surface. Data were acquired in constant analyzer energy (CAE) mode with a pass energy of 100 eV for survey spectra and 20 eV for high–resolution spectra. All spectra were charge–corrected by referencing the C 1s hydrocarbon peak to 284.80 eV. Surface elemental compositions were calculated using standard Scofield photoemission cross sections.

Circular dichroism (CD) spectra were recorded using a JASCO J–1500 spectropolarimeter equipped with a PM–539 detector and a PTC–517 temperature–controlled cell holder. Measurements were carried out in the 190–280 nm range with a 0.5 nm data pitch, 1.00 nm bandwidth, and a 4 s integration time. Spectra were acquired in CD, HT, and absorbance modes with 2–3 accumulations at 23.2–23.4 °C, using CA as the solvent.

Elemental analysis was carried out to determine the carbon, hydrogen, nitrogen, and sulfur contents (expressed as weight percentages) using a Truspec Micro CHNS 630–200–200 elemental analyzer. Approximately 1 mg of sample was used for each measurement. The combustion furnace was set to 1075 °C, and the afterburner operated at 850 °C. Carbon, hydrogen, and sulfur were quantified by infrared absorption, while nitrogen was measured using a thermal conductivity detector.

Thermogravimetric Analysis (TGA) was performed using a NETZSCH STA 409 PC/PG instrument. Approximately 8 mg of raw CFs and CFs after Pd adsorption (from tests with synthetic Pd mono–metallic solution containing (15 ± 1) $mg.L^{-1}$ of Pd) were placed in an alumina crucible. Tests were carried out under a nitrogen gas purge of 50 $mL.min^{-1}$. The temperature was ramped from 50 °C to 900 °C at a heating rate of 10 $K.min^{-1}$.

1.3. *Probing the Role of Amino and Disulfide Groups in Pd Adsorption*

To identify the involved functional groups in Pd adsorption, two tests were performed, in which amino groups and disulfide bonds were deactivated. Pd adsorption tests by CF were performed with a solution containing 15 $mg.L^{-1}$ of Pd, with pH adjusted at 5. At this pH, due to isoelectric point of CF (4.4 (Škerget et al., 2023)), amino groups are neutral and not positively charged, therefore cannot have a role in Pd adsorption. In the next test, CF were subjected to a chemical treatment designed to cleave disulfide linkages and cap the resulting thiol groups. Initially, CF were immersed in a solution containing 8 M urea and 100 mM dithiothreitol (DTT) at pH 8.5. The mixture was stirred at 50 °C for 6 h to reduce and cleave disulfide bonds. Following the reduction, iodoacetamide (IAM) was added to the solution at a final concentration of 250 mM to alkylate the free thiol groups, thereby preventing reformation of disulfide bonds. This reaction was conducted in the dark to avoid light–induced degradation or side reactions. After 1 h of incubation, cold ethanol (–20 °C) was added at a 1:3 volume ratio (sample:ethanol) to precipitate the protein material. The mixture was kept at –20 °C for 1 h, followed by centrifugation to collect the precipitate. The resulting pellet was washed three times with acetone to remove residual reagents and solvents. The final pellet, consisting of treated CF with capped thiol groups, was dried and subsequently used in Pd adsorption experiments.

1.4. *Desorption studies*

CF containing PGM, obtained under optimized adsorption conditions (0.2 M HCl, 303 K, and a 6–h contact time), were used in these experiments. To determine the total metal loading of CF after adsorption, a known mass of the CF sample was dissolved in aqua regia, and the concentrations of Fe, Zn, Ce, Pt, Pd, and Rh in the resulting solution were quantified (in triplicate). Subsequently, metal desorption from the same CF was performed using various desorption agents, including HCl (0.5, 1.0, 2.0, and 3.0 M), NaOH (0.5, 1.0 and 2.0 M), thiourea (0.2, 0.5, and 1.0 M) in 0.05 M HCl, and 0.2 M thiourea combined with HCl (0.03, 0.2, and 0.5 M). These tests were performed in triplicate at 303 K, at 150 rpm, and for 6 h. Finally, samples were filtered, and concentrations of metals were analyzed.

The desorption efficiency (D %) of each metal was then calculated as the percentage of the total adsorbed metal released into solution by each desorption agent, using the Equation S1:

$$D(\%) = \frac{C_d\, V_d}{q_{ads}\, m} \times 100 \qquad \text{(Eq. S1)}$$

where C_d ($mg.L^{-1}$) is the concentration of metal in the desorption solution, V_d (L) is the volume of the desorption solution, q_{ads} ($mg.g^{-1}$) is the amount of metal previously adsorbed on the adsorbent, and m (g) is the mass of the adsorbent used.

2. Results and discussion

2.1. CF particle size distribution and zeta potential

Laser–diffraction analysis of the ground CF showed a broad particle–size distribution, with a median diameter (D50) of 330 µm and wide spread (D10 = 33 µm; D90 = 756 µm), indicating the heterogeneous fragmentation produced by mechanical grinding. The full distribution curve and numerical parameters are presented in Figure S1.

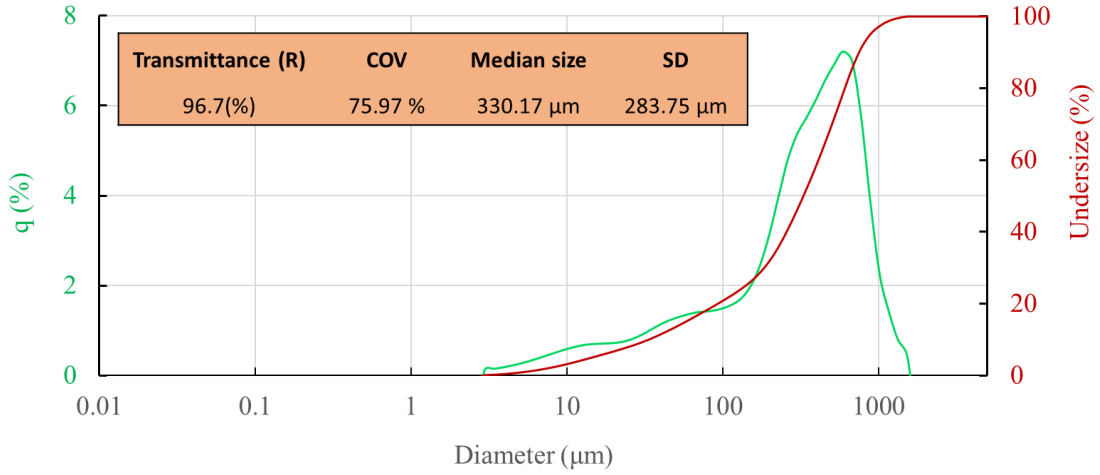

Figure S1. Particle size distribution of ground CF used in this study, measured by laser scattering. Median diameter = 330 µm; D10 = 33 µm; D90 = 755 µm.

CF showed positive zeta potentials (Figure S2) at low pH (from +6 to +10 mV at pH 1.8–2.6), became near neutral around pH 4.3–4.4, and shifted to strongly negative values above pH 5 (−25 to −35 mV).

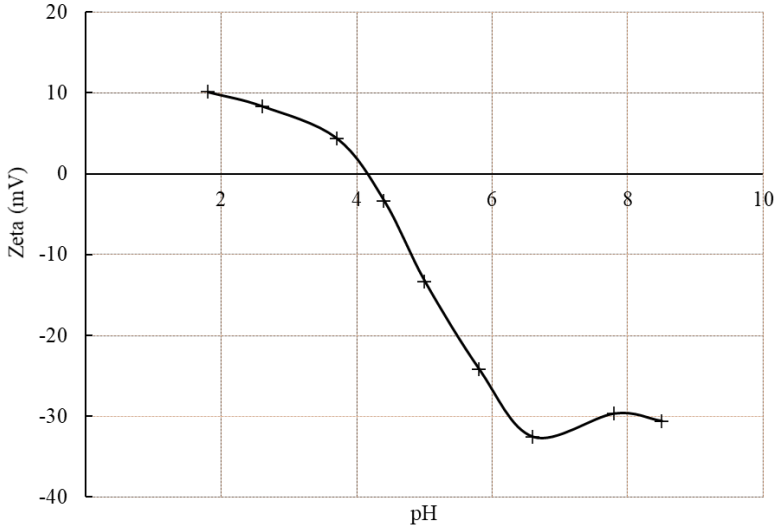

Figure S2. Zeta potential of CF as a function of pH.

2.2. *Adsorption kinetics*

Table S1. Kinetic parameters obtained from nonlinear pseudo–first–order, pseudo–second–order, and Weber–Morris intraparticle diffusion (IPD) models for the adsorption of Pd, Pt, and Rh onto CFs, along with their corresponding correlation coefficients (R^2).

		Pd	**Pt**	**Rh**
	$q_{e,\,exp}$ (mg.g^{-1})	14.67 ± 0.45	3.22 ± 0.14	1.61 ± 0.07
Pseudo–first order model	$q_{e,\,cal}$ (mg.g^{-1})	13.98	3.11	1.46
	R^2	0.97	0.96	0.94
	k_1 (min^{-1})	0.060	0.032	0.004
Pseudo–second order model	$q_{e,\,cal}$ (mg.g^{-1})	14.70	3.32	1.64
	R^2	0.99	0.97	0.97
	k_2 (g.mg^{-1}.min^{-1})	0.006	0.004	0.003
Weber–Morris model	k_1 (mg.L^{-1}.s$^{-1/2}$)	2.06	0.35	0.01
	R^2	0.98	0.86	0.86
	k_2 (mg.L^{-1}.s$^{-1/2}$)	0.04	0.01	0.02
	R^2	0.58	0.30	0.95

2.3. *Effect of initial metal concentration*

Table S2. Isotherm model parameters obtained from fitting experimental data of Pd and Pt adsorption onto CFs.

Model	Parameter	Pd	Pt
Langmuir	q_{max} (mg.g^{-1})	19.61	3.13
	K_L (L.mg^{-1})	2.57	0.98
	R^2	0.98	0.91
	R_L	0.03–0.16	0.04–0.22
Sips	q_{max} (mg.g^{-1})	18.85	4.11
	K_S (L.mg^{-1})	2.72	0.52
	n	1.46	0.44
	R^2	0.96	0.88
Temkin	K_T (L.g^{-1})	61.97	75.30
	b_T	6057.90	847.11
	R^2	0.94	0.88
Freundlich	K_F (mg.g^{-1})(L.mg^{-1})$^{1/n}$	11.68	1.93
	n	4.81	5.54
	R^2	0.88	0.45

Furthermore, the separation factor (R_L), a dimensionless parameter, was calculated using the equation below:

$$R_L = \frac{1}{1 + K_L.C_0} \quad \text{Eq. (S2)}$$

where C_0 (mg.L^{-1}) is the initial concentration of adsorbate in the solution.

Table S3. Comparison of Pd adsorption performance of CF with previously reported low–cost bio–based adsorbents reported in acidic chloride media.

Adsorbent	Type / Source	Modification	Medium/ condition	q_{max} (mg.g^{-1})	Pd selectivity	Reuse	Reference
Chicken feathers	Biowaste (keratin)	Unmodified	0.2 M HCl pH 0.79	19.61	>Pt >>Rh, Ce, Zn and Fe	Non–reusable	This work
Wool	Wool fabric	Chlorine–treated	pH 1	24.3	>Pt and Rh>> Cu, Ni	Non–reusable	(Akioka et al., 2021)
Fungal biomass	*Aspergillus* sp.	Unmodified	0.1 M HCl	4.3	Pt > Pd	5 cycles	(Godlewska–Żyłkiewicz et al., 2019)
Terrestrial moss	*Racomitrium lanuginosum*	Unmodified	pH 5	37.2	Not reported	Non–reusable	(Sari et al., 2009)
Silica–alginate nanomaterial	sodium alginate + silica	Crosslinked with silicate	pH 3	12.5	>>Y^{3+}, La^{3+}, Cd^{2+}, Co^{2+}, Sr^{2+}, Cs^{+}	Reusable	(Abd–Elhamid et al., 2023)
Chitin	Chitin waste	Unmodified	0.1 M HCl	2.8	Very low Pd affinity	Non–reusable	(Wang et al., 2021)
		Crosslinked with polyethylenimine		57.1	Not reported	3 cycles	
Thiourea–modified chitosan	Deacetylated chitin	Crosslinked with glutaraldehyde, grafted with thiourea	pH 2	112.4	Pt ≈ Pd ≫ Cu, Zn , Pb, Cd and Ca	5 cycles	(Zhou et al., 2009)
Activated carbon	Commercial activated carbon	None (used as–received)	0.1 M HCl	42.4	Not reported	2 cycles	(Wojnicki et al., 2018)
			pH 0	30		≥ 3 cycles	(Zhang et al., 2023)

Thiazole–modified activated carbon	Commercial activated carbon	Grafted with 2–aminothiazole	pH 3	150	≫ Zn, Fe, Cd, Mn, Li, Co and Ni

174

175 **Table S4.** Comparison of Pd adsorption capacities of CF with commercial synthetic sorbents reported in acidic chloride media.

Adsorbent	**Medium/ condition**	**q_{max} (mg.g^{-1})**	**Pd selectivity**	**Reuse**	**Reference**
Chicken feathers	0.2 M HCl	19.61	>Pt >>Rh, Ce, Zn and Fe	Non–reusable	This work
Lewatit MonoPlus SR–7	0.1 M HCl	197	≫ Fe^{3+} ≈ Cu^{2+} ≈ Ni^{2+} ≈ Zn^{2+} ≈ Pb^{2+} ≈ Co^{+} ≈ Ca^{2+} ≈ Na^{+}	≥ 5 cycles	(Wołowicz and Hubicki, 2012)
Varion ADAM	0.8 M HCl + 0.2 M HNO3	9.86	≫ base metals	Reusable	(Hubicki et al., 2009)
Lewatit MonoPlus MP600	Industrial HCl leachate	55	Pt > Pd ≫ Rh ≫ base metals	Reusable	(Goc et al., 2024a)
Puromet MTS 9200		51	> Pt ≫ Rh ≫ Zn^{2+}, Ni^{2+}, Fe^{3+} (Cu strongly competes)	Reusable	
Puromet MTS 9850		97	Pt ≈ Pd ≫ Rh ≫ base metals	Reusable	
Lewatit MonoPlus TP 214	0.1 M HCl	241	≫ base metals	Non–reusable	(Won and Yun, 2013)

Chelite S	0.1 M HCl	260	≫ base metals	Reusable	(Zbigniew Hubicki and Wołowicz, 2009)
Amberlyst A21	0.1 M HCl + 1 M NaCl	27.9	≫ base metals	Reusable	(Z. Hubicki and Wołowicz, 2009)

176

2.4. Effect of HCl concentration

The distribution coefficient (K_d) for each metal was determined from the ratio between its concentration change in solution and the amount of adsorbent used. K_d was calculated using:

$$K_d = \frac{C_0 - C_e}{C_e} \times \frac{V}{m} \quad \text{(Eq. S3)}$$

where C_0 and C_e ($mg.L^{-1}$) are the initial and equilibrium metal concentrations, V (L) is the solution volume, and m (g) is the mass of adsorbent.

Selectivity coefficients (K) between Pd and other metals were obtained by taking the ratio of their distribution coefficients:

$$K_{Pd/Me} = \frac{K_{d,Pd}}{K_{d,Me}} \quad \text{(Eq. S4)}$$

Values greater than 1 indicate preferential adsorption of Pd over other metals.

Table S5. HCl concentration effect on the distribution coefficient (K_d) and selectivity coefficient (K) of tested metals.

	HCl conc. (M)	Metal					
		Pd	**Pt**	**Rh**	**Ce**	**Zn**	**Fe**
K_d ($L.g^{-1}$)	**0.04**	34.23	0.91	0.22	8.37×10^{-3}	3.90×10^{-4}	8.70×10^{-4}
	0.1	26.26	0.53	0.15	7.09×10^{-3}	2.72×10^{-3}	7.82×10^{-3}
	0.2	26.55	0.36	9.86×10^{-2}	8.60×10^{-3}	6.00×10^{-3}	4.45×10^{-3}
	0.5	1.09	0.10	3.52×10^{-3}	1.16×10^{-2}	1.39×10^{-2}	7.26×10^{-3}
	1	0.72	0.04	8.32×10^{-4}	4.18×10^{-3}	4.92×10^{-3}	3.73×10^{-3}
	2	0.47	0.01	3.93×10^{-4}	4.46×10^{-3}	1.63×10^{-3}	2.33×10^{-3}
K	**0.04**	–	37.48	155.57	4.09×10^{3}	8.78×10^{4}	3.94×10^{4}
	0.1	–	49.46	172.08	3.70×10^{3}	9.66×10^{3}	3.36×10^{3}
	0.2	–	74.76	269.21	3.09×10^{3}	4.43×10^{3}	5.96×10^{3}
	0.5	–	11.19	309.88	94.17	78.28	150.32
	1	–	16.21	860.87	171.24	145.50	192.12
	2	–	54.54	1.19×10^{3}	105.04	287.69	201.26

Table S6. H_2SO_4 and HNO_3 concentration effect on the distribution coefficient (K_d) and selectivity coefficient (K) of tested metals.

	Acid conc. (M)	Metal					
		Pd	**Pt**	**Rh**	**Ce**	**Zn**	**Fe**
	H_2SO_4						
K_d ($L.g^{-1}$)	**0**	20.59	0.52	0.14	8.59×10^{-3}	5.97×10^{-3}	4.44×10^{-3}
	0.2	3.72	0.12	9.74×10^{-4}	1.19×10^{-2}	3.72×10^{-3}	3.96×10^{-3}
	0.5	2.72	0.07	3.47×10^{-3}	1.67×10^{-2}	1.06×10^{-2}	1.79×10^{-2}
	1	1.81	0.06	6.16×10^{-3}	1.11×10^{-2}	1.63×10^{-3}	2.44×10^{-3}
$K_{dPd/met}$	**0**	–	39.72	148.93	2.40×10^{3}	3.45×10^{3}	4.64×10^{3}

	0.2	–	32.00	3.82×10^{3}	312.55	1.00×10^{3}	940.95
	0.5	–	36.64	783.28	162.96	256.10	151.72
	1	–	29.31	294.46	163.38	1.11×10^{3}	742.55
	HNO_3						
K_d ($L.g^{-1}$)	**0**	20.59	0.52	0.14	8.59×10^{-3}	5.97×10^{-3}	4.44×10^{-3}
	0.2	1.97	0.12	1.14×10^{-3}	2.04×10^{-2}	1.80×10^{-2}	5.10×10^{-2}
	0.5	1.46	7.33×10^{-2}	6.97×10^{-3}	4.08×10^{-2}	2.94×10^{-2}	7.63×10^{-3}
	1	1.15	5.48×10^{-2}	4.92×10^{-3}	1.96×10^{-2}	1.00×10^{-2}	7.56×10^{-3}
K	**0**	–	39.72	148.93	2.40×10^{3}	3.45×10^{3}	4.64×10^{3}
	0.2	–	16.40	1.73×10^{3}	96.64	109.33	38.57
	0.5	–	19.95	209.89	35.81	49.79	191.51
	1	–	20.90	232.95	58.58	114.05	151.57

To verify whether the reduced Pd adsorption capacity observed in 2 M HCl is caused by structural damage or alteration of functional groups in CFs at high acid concentrations, a control test was conducted. CFs (1 $g.L^{-1}$) were immersed in 2 M HCl and agitated for 6 h. The treated CFs were then separated, thoroughly washed with deionized water, and dried in an oven at 50 °C overnight. Subsequently, these pre–treated CFs were used for adsorption from a synthetic multimetallic solution containing (15 ± 1) $mg.L^{-1}$ of Pd, Pt, Rh, Fe, Zn, and Ce in 0.2 M HCl. The results showed no significant difference compared to untreated CFs, indicating that the decline in adsorption capacity at higher HCl concentrations is not attributable to structural degradation or modification of CF functional groups (Figure S3).

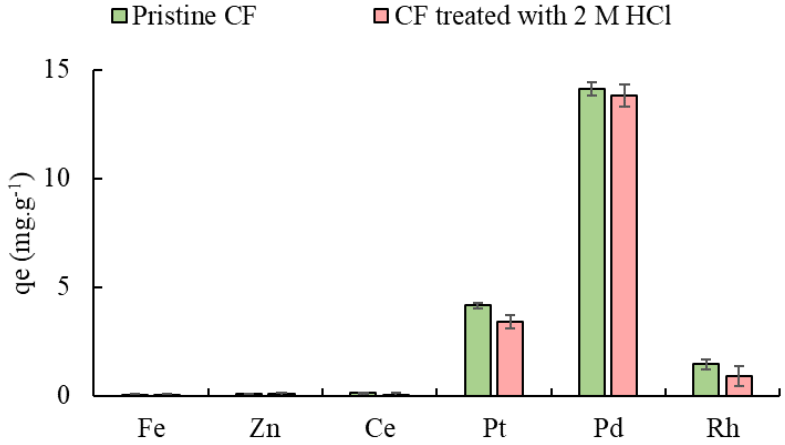

Figure S3. Metal adsorption behavior of pristine and 2 M HCl–treated CF from a multimetallic solution in 0.2 M HCl.

2.5. Effect of competitive metal ions

The effect of competitive metal ion concentrations on Pd adsorption by CF was evaluated by systematically increasing the concentrations of one of competitive metals (Fe, Zn, Ce, Pt or Rh) tenfold ((150 ± 5) $mg.L^{-1}$) while maintaining the concentration of other metals at (15 ± 1) $mg.L^{-1}$ (Figure S4). Results demonstrated that in all tests, Pd consistently achieved the highest adsorption levels compared to other metals. However, by comparing the adsorption uptake in these tests with the control, a measurable decline in Pd adsorption capacity was observed in tests with tenfold Pt and Rh concentrations, accompanied by an increase in their adsorption capacities (Figure S4). This behavior is attributed to the negatively charged chloride complexes of Pt and Rh, which compete with Pd for adsorption sites on CF. At elevated Pt or Rh concentrations, mass action effects become more pronounced, facilitating their adsorption despite their potentially lower intrinsic affinity, ultimately leading to higher adsorption rates than in the unspiked samples. This antagonistic interaction highlights the competitive nature of adsorption and the site–blocking effects that influence metal distribution on adsorbent surfaces.

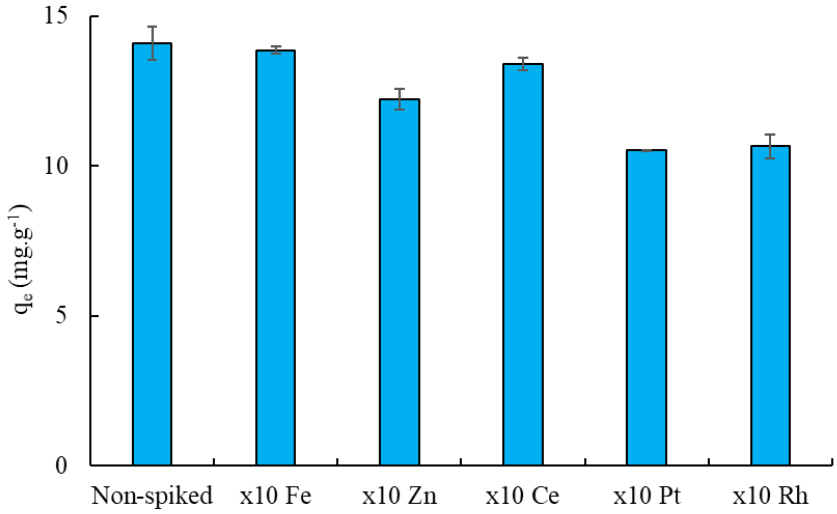

Figure S4. Adsorption variation of Pd following a 10–fold increase in competitive metal concentration. CF dosage of 1 $g.L^{-1}$, initial concentrations of each metal at (15 ± 1) $mg.L^{-1}$, concentration of spiked metal at 150 ± 5 $mg.L^{-1}$, HCl concentration of 0.2 M, temperature at 303 K, and a contact time of 360 min.

Moreover, as shown in Figure S4, a tenfold increase in Zn concentration resulted in a slight but noticeable decrease in Pd and Pt adsorption capacities, along with the sorption of a small amount of Zn (1.8 $mg.L^{-1}$) from the solution. This suggests that at elevated Zn concentrations, despite not forming strongly adsorbing anionic complexes like Pd and Pt at the studied HCl concentration, Zn may still weakly interact with the CF surface, possibly through subtle complexation (Mishra, 2014). These secondary interactions effectively reduce the availability of active sites for Pd and

Pt, thereby hindering their uptake. In contrast, similar increases in Fe and Ce concentrations had minimal impact on Pd and Pt adsorption capacities, highlighting that the unique speciation and behavior of Zn under the given conditions play a distinct role in influencing the adsorption process.

2.6. Adsorption mechanism

To assess the practicability and nature of the adsorption process, thermodynamic parameters, including enthalpy change, $\Delta H\ (J.mol^{-1})$, entropy change, $\Delta S\ (J.mol^{-1})$, and Gibbs free energy change, $\Delta G\ (J.mol^{-1})$, were analyzed. These parameters were derived using the Van't Hoff equation (Eq. S5):

$$lnK = -\frac{\Delta H}{RT} + \frac{\Delta S}{R} \qquad \text{Eq. (S5)}$$

Here K is the dimensionless thermodynamic equilibrium constant, T is the absolute temperature (K), and R is the universal gas constant (8.314 $J.mol^{-1}.K^{-1}$). The adsorption equilibrium constant was initially estimated using the distribution coefficient, K_d ($L.g^{-1}$), defined as:

$$K_d = \frac{q_e}{C_e} \qquad \text{Eq. (S6)}$$

where q_e is the equilibrium adsorption capacity ($mg.g^{-1}$) and C_e is equilibrium concentration of the solute in the solution ($mg.L^{-1}$). However, the direct use of K_d as a thermodynamic equilibrium constant is problematic due to its dimensional nature and lack of physical significance, as highlighted by Tran (2022). To address this, a dimensionless equilibrium constant (K) was derived by incorporating the standard adsorbent concentration (1 $g \cdot L^{-1}$):

$$K = K_d \times adsorbent\ dose\ (g.L^{-1}) \qquad \text{Eq. (S7)}$$

And ΔG was determined from the Equation S8:

$$\Delta G = -RTlnK \qquad \text{Eq. (S8)}$$

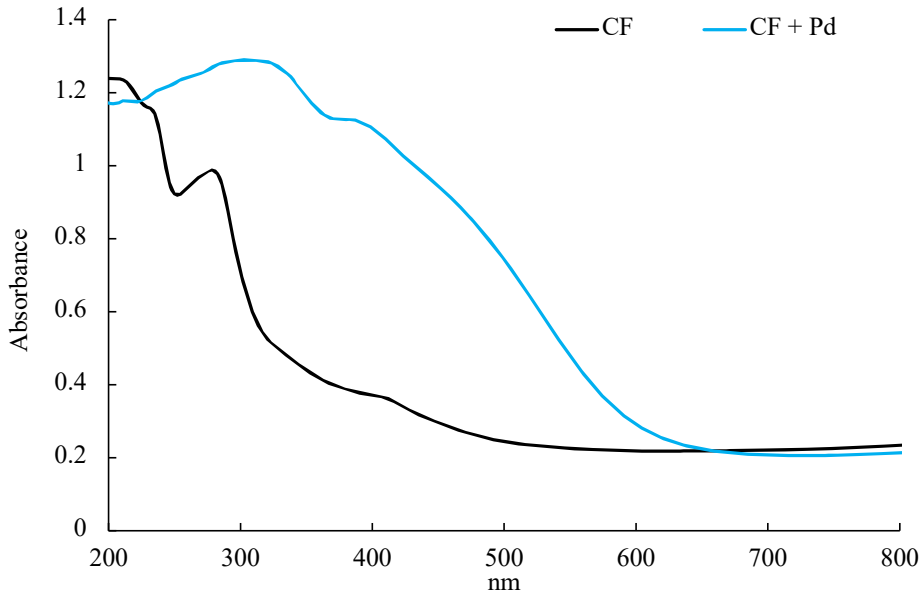

Figure S5. Solid–phase UV–visible spectroscopy of CFs before and after Pd adsorption.

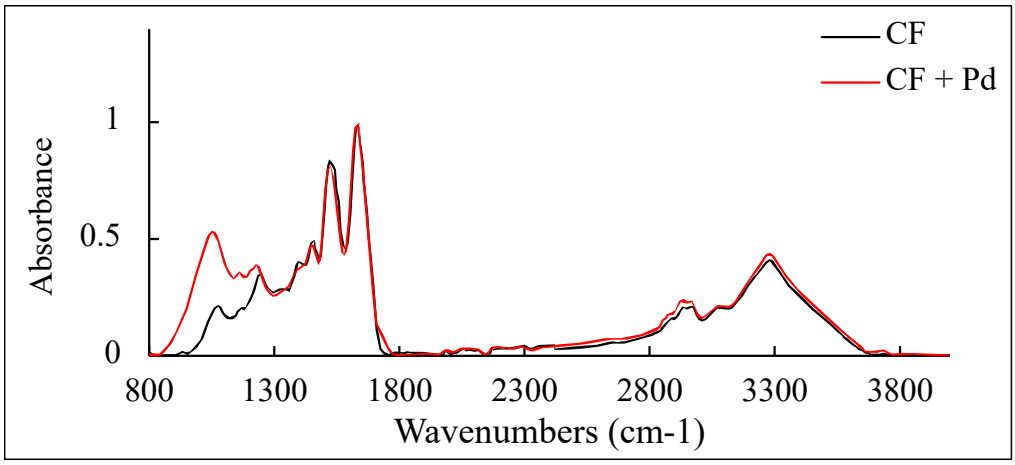

Figure S6. FTIR spectra of CFs before and after Pd adsorption from a 100 mg/L Pd solution in 0.2 M HCl by 1 g.L^{-1} CFs. CF dosage of 1 g.L^{-1}, temperature at 303 K and a contact time of 360 min.

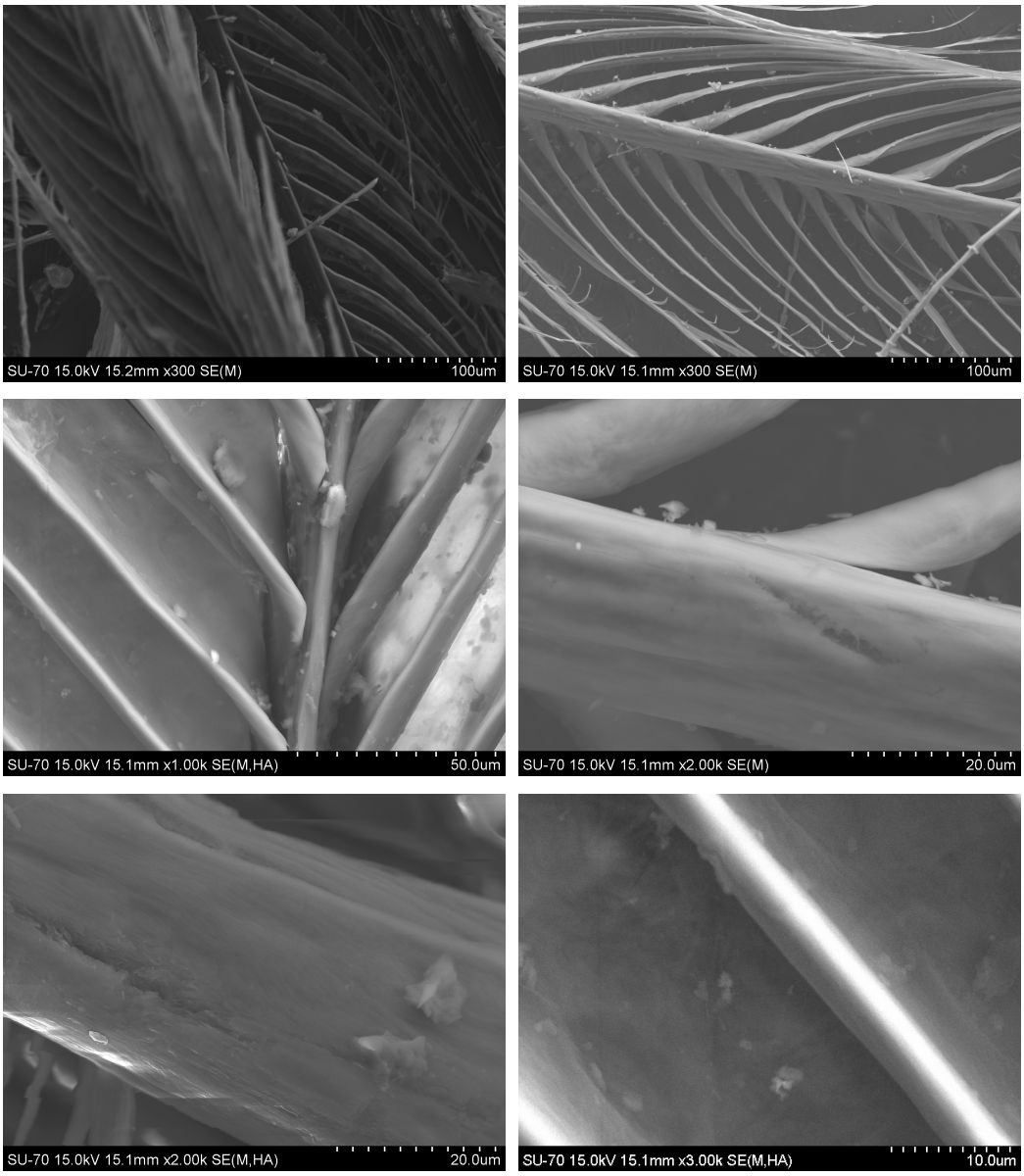

Figure S7. SEM images of CFs after the adsorption process from MixC 1/6 (v/v) leachate.

Table S7. Normalized elemental abundances of CFs before and after Pd adsorption from 100 mg.L^{-1} synthetic solution in 0.2 M HCl, determined by SEM–EDX from the highlighted area in Figure 4–B.

	Raw CFs		After Pd adsorption	
Element	[norm. wt.%]	[norm. at.%]	[norm. wt.%]	[norm. at.%]
Cl	0.09	0.04	3.34	1.32
S	4.00	1.68	4.17	1.82
C	55.36	62.03	55.58	64.92
O	22.44	18.88	20.07	17.60
N	18.07	17.36	13.92	13.94
Pd	0.04	0.01	2.92	0.39
Sum	100	100	100	100

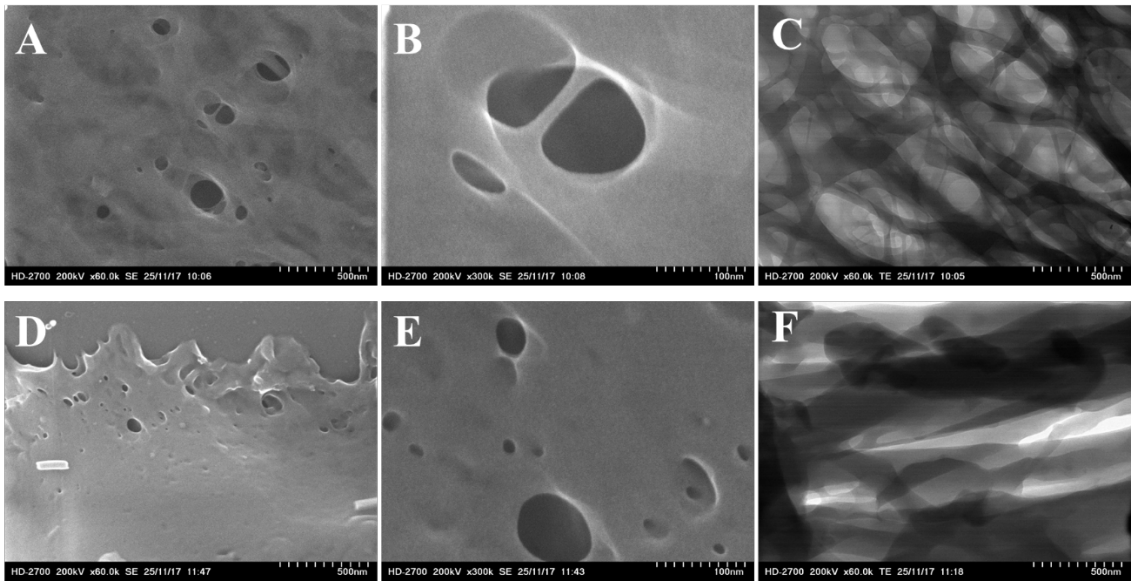

Figure S8. (A, B) STEM surface and (C) transmission images of untreated CF, and (D, E) surface and (F) transmission images of CF after Pd adsorption from the multimetallic solution with 2 M HCl.

Table S8. Surface elemental composition (At. %) of the CFs before and after Pd adsorption and also after Pd desorption by 0.2 M TU + 0.5 M HCl, as determined by XPS analysis.

Sample	XPS Surface Elemental Quantitation (At. %)					
	C	O	N	S	Pd	Cl
CF	77.3	12.82	8.79	1.1	–	–
CF + Pd	78.1	11.78	6.13	0.98	0.52	2.48
CF after Pd desorp.	73.56	13.0	9.0	1.23	–	0.31

Table S9. Binding energy and relative abundance % of CFs before and after Pd adsorption, and also after Pd desorption by 0.2 M TU + 0.5 HCl.

	CFs		CFs + Pd		CFs after Pd desorp.		Correlated groups
	BE (eV)	RA (%)	BE (eV)	RA (%)	BE (eV)	RA (%)	
C 1s	284.8	53.10	284.8	46.26	284.8	44.71	C–C, C–H_x
	286.3	19.47	286.3	22.53	–	–	C–N, C–O–C, C–O–H, C–Cl
	–	–	–	–	287.6	41.14	C=O–N
	288.1	18.72	288.1	19.17	–	–	C=O, N–C=O
	289.9	5.48	290.3	12.03	–	–	O=C–O
	291.6	3.23	–	–	291.4	14.15	
O 1s	–	–	529.8	27.84	–	–	Metal–O
	531.5	59.28	531.4	46.55	531.7	51.56	C=O
	533.0	34.17	533.8	15.22	533.8	24.14	O–**C**–O, **C**–OH
	535.4	6.55	535.9	10.39	535.9	15.55	
	–	–	–	–	538.9	8.76	
N 1s	399.2	6.96	399.3	13.51	398.8	5.95	C–N–C
	400.4	37.25	400.5	52.93	400.0	78.96	–NH_2
	401.9	37.58	401.7	25.51	401.3	15.09	Protonated amine or amide
	403.4	18.20	403.1	8.05	–	–	N–O
S 2p	163.7	83.92	163.8	75.08	163.9	45.22	S–S

	164.8	0.00	165.1	0	165.2	0	
	167.6	16.08	167.6	24.92	167.3	27.8	Oxidized S
	168.9	0.00	168.9	0.00	168.4	0	
	–	–	–	–	170.6	26.98	
	–	–	–	–	171.9	0	
Pd 3d	–	–	338.05	100	–	–	Pd^{2+}
			343.1	0			
Cl 2p	–	–	198.57	78.77	–	–	

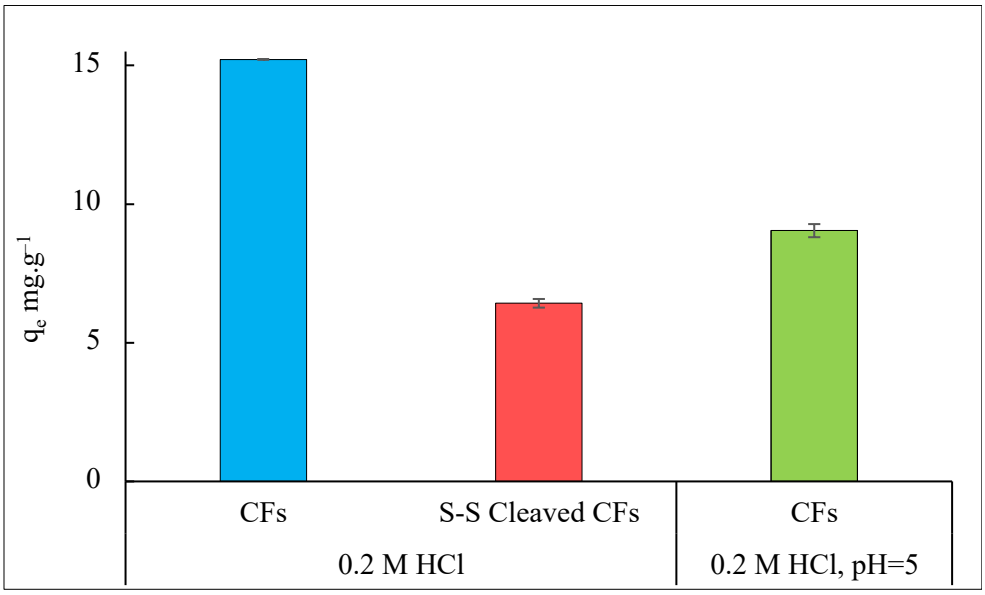

Figure S9. Percentage recovery of Pd from a solution containing (15 ± 1) mg·L^{-1} Pd in 0.2 M HCl using untreated CFs, disulfide–cleaved CFs, and from a solution adjusted to pH 5 using untreated CFs.

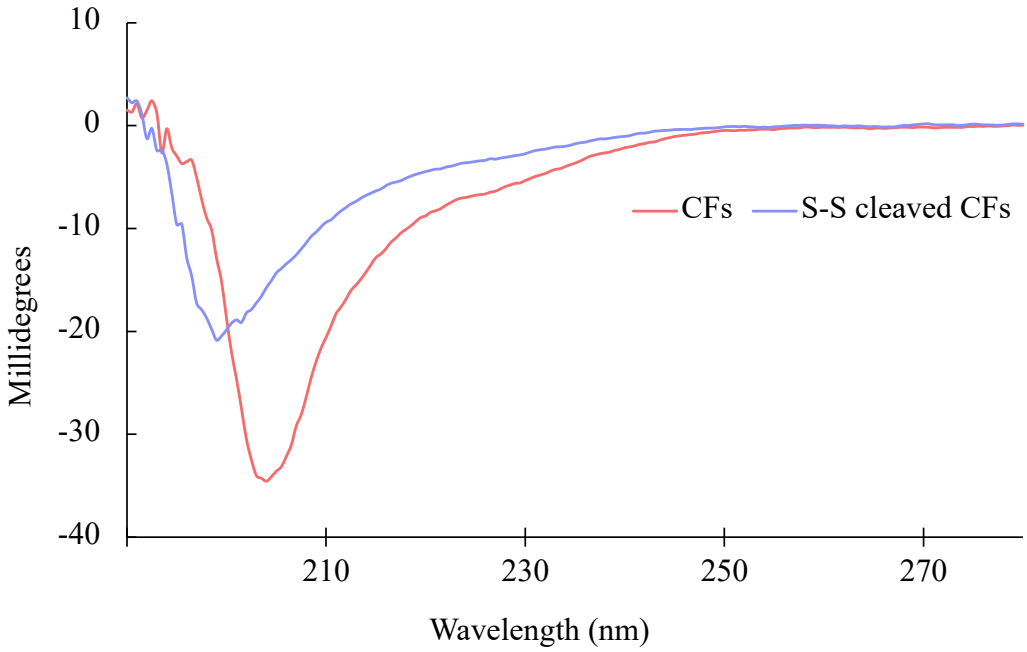

Figure S10. Circular dichroism (CD) spectra of CFs before and after disulfide bond cleavage.

2.7. Desorption

Feathers with adsorbed metals, obtained at optimized conditions from tests with synthetic solutions were initially digested in aqua regia, revealing metal loadings of (14.82 ± 0.32), (4.70 ± 0.25) and (2.07 ± 0.08) $mg.g^{-1}$ of Pd, Pt and Rh, respectively. Subsequent desorption experiments were conducted using various molarities of HCl, NaOH, and thiourea (TU) (Figure S11). Results from desorption with HCl indicated a degree of selectivity toward Pt desorption over Pd (Figure S11–A). At lower HCl concentrations (0.5 and 1.0 M), approximately 70 % (~3.3 $mg.g^{-1}$) of the adsorbed Pt was desorbed, while Pd removal remained low at only 5–8 % (~0.74–1.18 $mg.g^{-1}$). Increasing the HCl concentration to 2.0 and 3.0 M enhanced Pt desorption to 84% and 99%, though Pd desorption also rose to about 18% and 26%. By contrast, NaOH solutions, tested at 0.5, 1.0, and 2.0 M (Figure S11–B), consistently demonstrated low desorption efficiencies for both Pd and Pt. Notably, Rh remained bound under both HCl and NaOH conditions, with no detectable desorption observed.

Parallel experiments were conducted using solutions with various concentrations of TU in acidified media containing 0.05 M HCl. Acidification is essential as it enhances TU–metal complex formation through TU protonation (Ammi Said et al., 2013). These studies revealed higher desorption efficiencies for all three metals with low TU concentrations (0.2 M) (Figure S11–C). It is known that low TU levels promote the formation of soluble Pd–TU complexes,

enhancing detachment from CF, while excessive TU can disrupt the equilibrium or increase viscosity, hindering metal release (Chatterjee and Abraham, 2019).

Further studies were performed to improve the desorption yield. For this purpose, 0.2 M TU was selected as fixed TU concentration in combination with varying HCl molarities (0.2, 0.5 and 1.0 M HCl) (Figure S11–D). Among these, the combination of 0.2 M TU and 0.5 M HCl demonstrated the highest efficiency, desorbing nearly 100 % of both Pd and Pt, along with approximately 90 % of Rh. The stripped Pd in the eluate can subsequently be recovered either by cementation with Zn powder, chemical reduction (Goc et al., 2024b), or precipitation with alkali metal borohydrides (Awadalla et al., 1990).

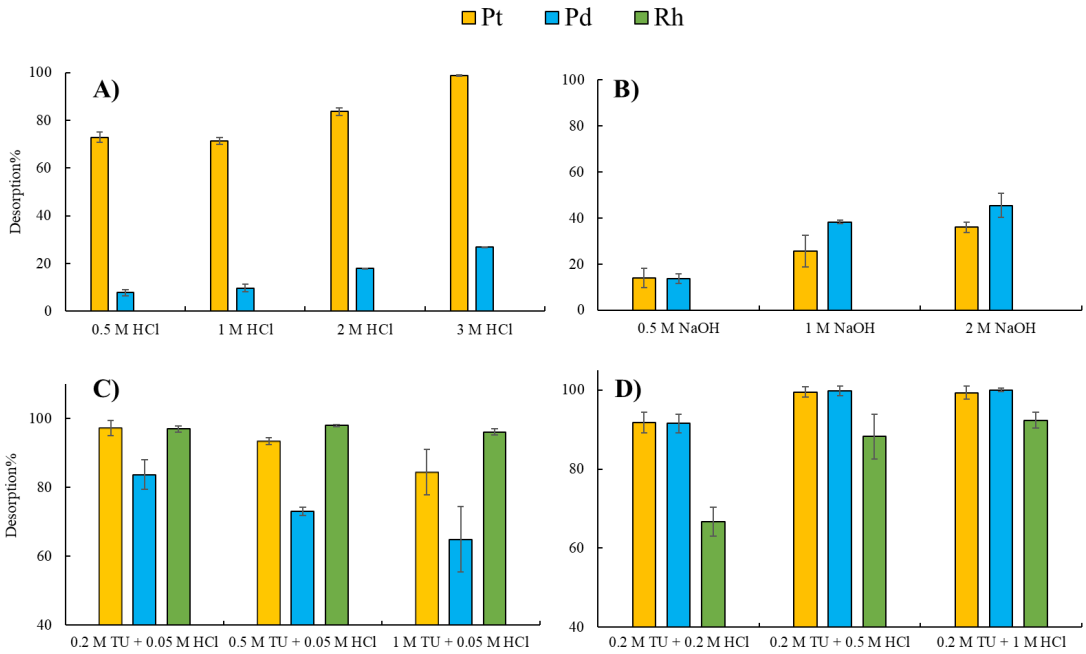

Figure S11. Desorption studies of Pd, Pt and Rh from PGM loaded CF, obtained from optimized adsorption studies by different concentrations of (A) HCl, (B) NaOH, (C) 0.2 TU + 0.05 M HCl and (D) 0.2 M TU + 0.5 HCl. (Total metal content of feathers before desorption: 4.69 $mg.g^{-1}$ of Pt, 14.82 $mg.g^{-1}$ Pd, and 2.07 $mg.g^{-1}$ Rh).

2.8. Desorption mechanistic studies

Based on the XPS analysis of pristine CF and after Pd adsorption–desorption (desorption by 0.2 M TU + 0.5 M HCl), notable structural and compositional changes are evident (Figure S12, Table S9 and Table S10). In the pristine CF, the surface exhibits typical signals corresponding to C, O, N, and S, reflecting the native protein structure of keratin. However, after Pd desorption, the elemental profile changes significantly. The S signal, which is critical for Pd binding via thiol and disulfide groups, is considerably diminished, indicating potential chemical alteration or oxidation

of these functional groups during the desorption process (Figure S12–C). Additionally, the possible loss or transformation of nitrogen–containing groups suggests that the chemical integrity of keratin is compromised. These alterations likely reduce the material's capacity for effective re–adsorption of Pd^{2+}. Despite no significant changes in the elemental composition of the CF before and after extraction (Table S10), the XPS data imply that CF after undergoing Pd desorption may not be suitable for reuse.

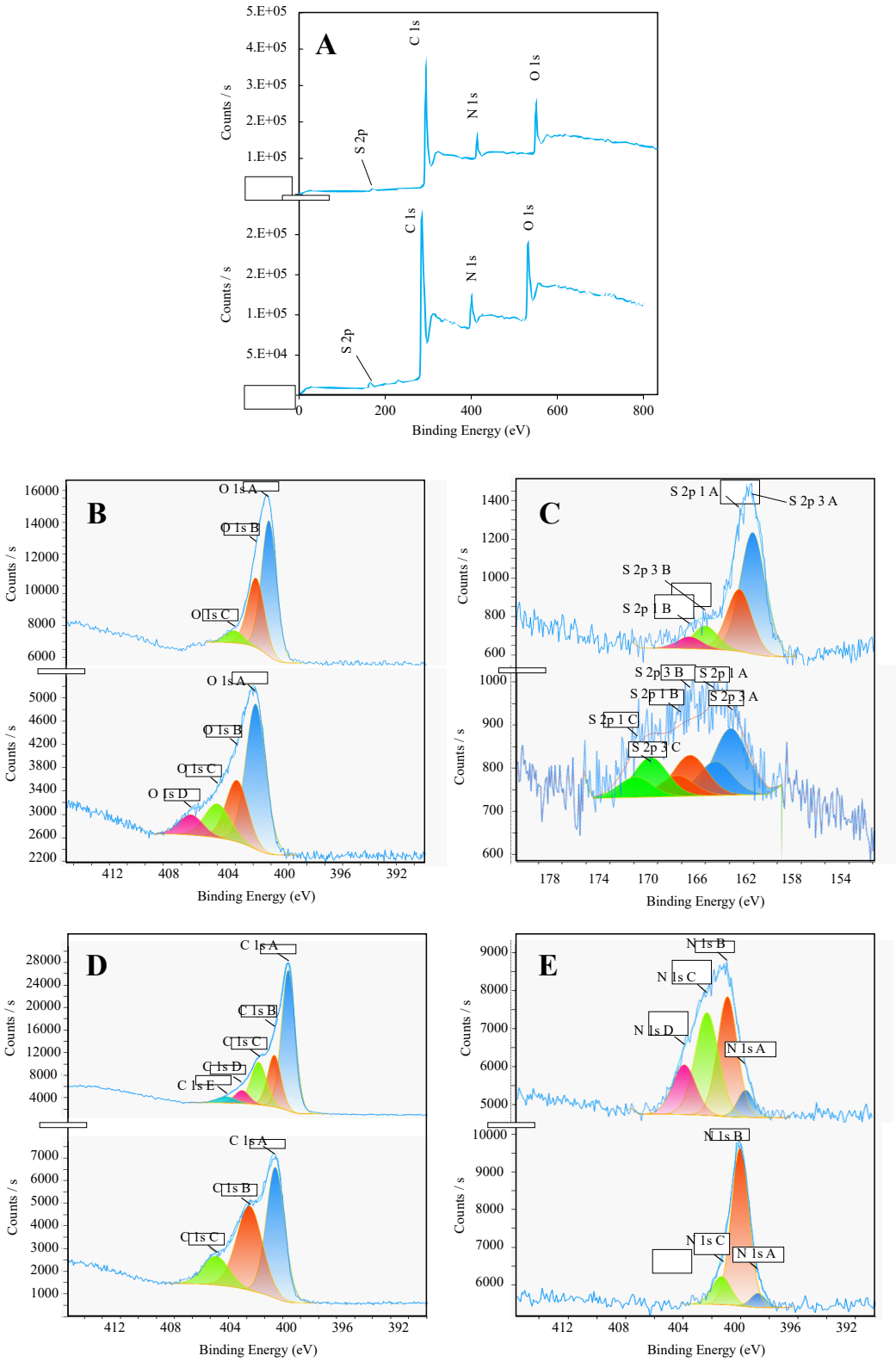

344

345 **Figure S12.** (A) Wide–scan XPS survey spectra; high–resolution XPS spectra of (B) O 1s, (C)
346 S 2p, (D) C 1s and (E) N 1s regions. Each panel shows spectra of pristine CFs (top) and after Pd
347 adsorption–desorption (bottom).

348

Table S10. CHNS elemental analysis of CFs before and after Pd adsorption, and following Pd desorption with 0.2 M TU + 0.5 M HCl.

Sample	Average			
	%C	%H	%N	%S
CF	46.67 ± 0.41	6.78 ±0.53	15.62 ± 1.61	2.58 ± 0.11
CF after Pd adsorption	46.93 ± 0.20	5.83 ± 0.52	14.94 ± 0.61	2.40 ± 0.11
CF after Pd desorption by TU–HCl	45.88 ± 0.88	6.18 ± 0.19	14.67 ± 0.37	2.34 ± 0.16

2.9. Leachate characterization

Table S11. Metal concentrations in the original (non–diluted), 1/6 and 1/60 (v/v) diluted leachates of VW90 and MixC (Leaching condition: 11.6 M HCl with 1% H_2O_2 at 70 °C for 3 h).

Metal ($mg.L^{-1}$)	VW90			MixC		
	Original	Diluted 1/6	Diluted 1/60	Original	Diluted 1/6	Diluted 1/60
Fe	115.6 ± 8.4	25.56 ± 1.33	2.4 ± 0.0	263.5 ± 14.3	42.0 ± 3.9	5.6 ± 0.0
Zn	74.6 ± 4.7	11.44 ± 0.74	1.5 ± 0.0	81.0 ± 2.4	12.2 ± 0.2	1.6 ± 0.0
Ce	3422.6 ± 36.1	630.83 ± 2.55	67.0 ± 0.8	2672.2 ± 28.7	445.7 ± 4.6	53.9 ± 2.0
Pt	14.6 ± 1.9	2.54 ± 0.31	0.5 ± 0.1	310.6 ± 5.9	39.2 ± 0.9	4.0 ± 0.0
Pd	1180.9 ± 20.5	167.14 ± 3.25	20.0 ± 0.9	538.9 ± 13.7	85.1 ± 2.2	8.5 ± 0.2
Rh	59.8 ±0.3	2.89 ± 0.05	0.5 ± 0.0	28.8 ± 2.1	4.8 ± 0.3	0.4 ± 0.0
Ti	350.0 ± 2.9	49.30 ± 0.47	0.7 ± 0.0	70.1 ± 0.8	5.1 ± 0.1	0.4 ± 0.0
Ni	18.5 ± 0.6	4.5 ± 0.1	0.5 ± 0.0	14.5 ± 0.4	3.2 ± 0.1	<LOD
Cu	36.5 ± 0.4	6.3 ± 0.1	0.98 ± 0.01	18.5 ± 0.2	3.6 ± 0.0	<LOD

2.10. Application to real leachates – optimization

Adsorption tests on real leachates were initially performed using leachates diluted to 1/60, with HCl concentration of ~0.2 M. Based on the maximum adsorption capacity of CFs measured at 0.2 M HCl ((19.61 ± 1.31) $mg.g^{-1}$; Table S2) and the Pd concentrations in VW90 and MixC leachates (20.04 and 8.50 $mg.L^{-1}$, respectively), it was determined that 1 $g.L^{-1}$ of CFs was theoretically sufficient to achieve complete Pd recovery from both solutions. Indeed, more than 95% of Pd was adsorbed from both leachates (Figure S13). Since the VW90 leachate has a negligible Pt concentration, no changes were observed after adsorption; whereas in the MixC leachate, approximately 50 % of Pt (~2 $mg.L^{-1}$) was recovered (Figure S13). Rh concentrations in both leachates were initially very low and remained largely unchanged.

On the other hand, in order to recover Pd from the 1/6 diluted leachates with HCl concentration of ~2 M, an "adjusted" maximum adsorption capacity ($q_{max,\ adjusted}$) of CFs was estimated from the maximum adsorption capacity and the decrease in Pd adsorption efficiency at 2 M HCl (33%; Figure 2–A). This calculation yielded a $q_{max,\ adjusted}$ of 6.47 $mg.g^{-1}$ of CFs in 2 M HCl solutions. Considering Pd concentration in 1/6 diluted VW90 (~167 $mg.L^{-1}$) and MixC (~85 $mg.L^{-1}$) leachates, a cumulative CF dosage of 25 $g.L^{-1}$ and 15 $g.L^{-1}$, respectively, were estimated to be sufficient for complete Pd recovery. Based on these estimates, five and three successive adsorption cycles, each with 5 $g.L^{-1}$ of fresh CFs, were conducted for VW90 and MixC leachates, respectively. In the VW90 leachate, Pd uptake by CFs progressively declined across five adsorption cycles, with adsorption capacities of 13.2, 8.0, 7.0, 3.2, and 1.2 $mg.g^{-1}$ CF, respectively (Table S12), equivalent to a total Pd adsorption of about 66, 40, 35, 16, and 6 $mg.L^{-1}$ by 5 g of CFs in each cycle. The maximum Pd adsorption capacity observed in the first cycle was nearly double the estimated $q_{max,\ adjusted}$ for this test, attributed to the combined effects of increased Pd concentration and the leachate's ionic strength. After five adsorption cycles, Pd was reduced below the detection limit. As illustrated in **Error! Reference source not found.** and Table S12, four adsorption cycles were sufficient to recover ~96% of Pd with very little contamination, especially during the first three cycles, reaching purities of approximately 99%. Only negligible amounts of Pt and Rh (total amount of 0.16 and 0.24 $mg.g^{-1}$, respectively) were adsorbed by CFs after four successive cycles (Table S12). No significant changes were observed in the concentrations of other metals throughout the study, this includes metals tested in optimization steps (Fe, Zn and Ce) and also other metals present in the leachate including Ti, Ni and Cu. Importantly, a similar result was obtained for the 1/6 diluted MixC leachate, confirming the robustness of the separation (Table S12).

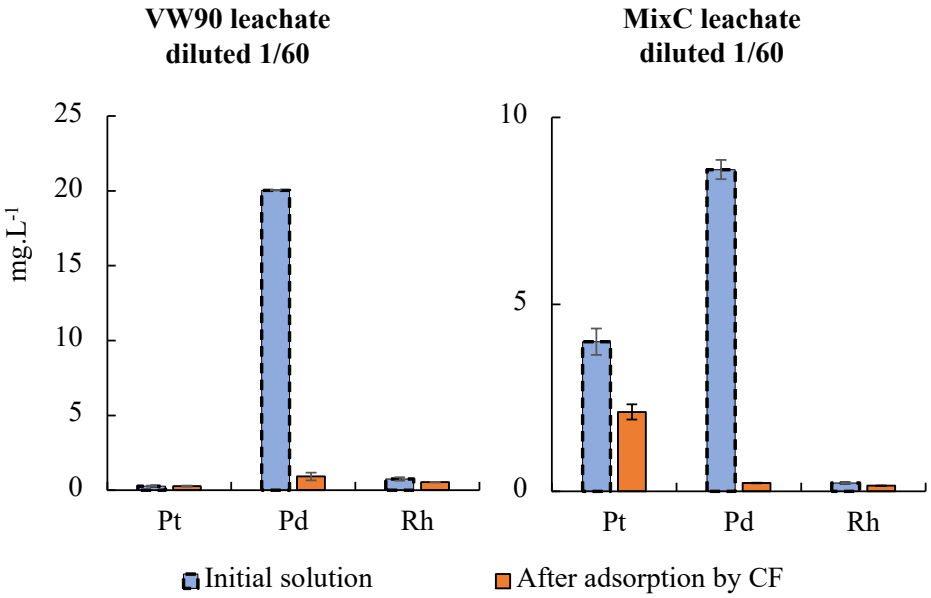

392

393 **Figure S13.** PGMs adsorption by 1 g/L of a) VW90 and b) MixC 1/60 (v/v) leachates. CF dosage
394 of 1 g.L^{-1}, temperature at 30 °C and a contact time of 360 min.

395

396 **Table S12.** Adsorption capacity of tested PGMs per gram of CFs from 1/6 diluted VW90 and
397 MixC leachates per adsorption cycles. CF dosage of 5 g.L^{-1} in each cycle, temperature at 303 K
398 and a contact time of 360 min.

Ads. cycle	C_e (mg.L^{-1})			q_e (mg.g^{-1})		
	Pt	**Pd**	**Rh**	**Pt**	**Pd**	**Rh**
	1/6 diluted VW90 leachate					
Before ads.	2.53 ± 0.07	163.52 ± 4.11	2.89 ± 0.03	–	–	–
1st cycle	2.50 ± 0.11	97.16 ± 1.96	2.89 ± 0.03	0.00 ± 0.01	13.27 ± 0.39	0.00 ± 0.00
2nd cycle	2.33 ± 0.11	57.20 ± 0.48	2.81 ± 0.03	0.03 ± 0.01	7.99 ± 0.10	0.02 ± 0.01
3rd cycle	1.85 ± 0.08	22.28 ± 2.96	2.71 ± 0.03	0.10 ± 0.02	6.98 ± 0.59	0.02 ± 0.01
4th cycle	1.73 ± 0.02	6.04 ± 1.26	1.75 ± 0.09	0.02 ± 0.02	3.25 ± 0.25	0.19 ± 0.02
5th cycle	0.61 ± 0.11	<LOD	1.45 ± 0.12	0.22 ± 0.02	1.21 ± 0.00	0.06 ± 0.01
	1/6 diluted MixC leachate					
Initial	39.14 ± 0.08	85.10 ± 1.27	4.86 ± 0.03	–	–	–
1st cycle	36.18 ± 0.28	37.03 ± 0.21	4.86 ± 0.03	0.59 ± 0.02	9.61 ± 0.04	0.00 ± 0.01
2nd cycle	33.86 ± 0.25	2.26 ± 0.07	3.19 ± 0.02	0.46 ± 0.05	6.95 ± 0.01	0.33 ± 0.00
3rd cycle	21.83 ± 0.78	<LOD	3.10 ± 0.00	2.41 ± 0.16	0.45 ± 0.00	0.07 ± 0.00

399

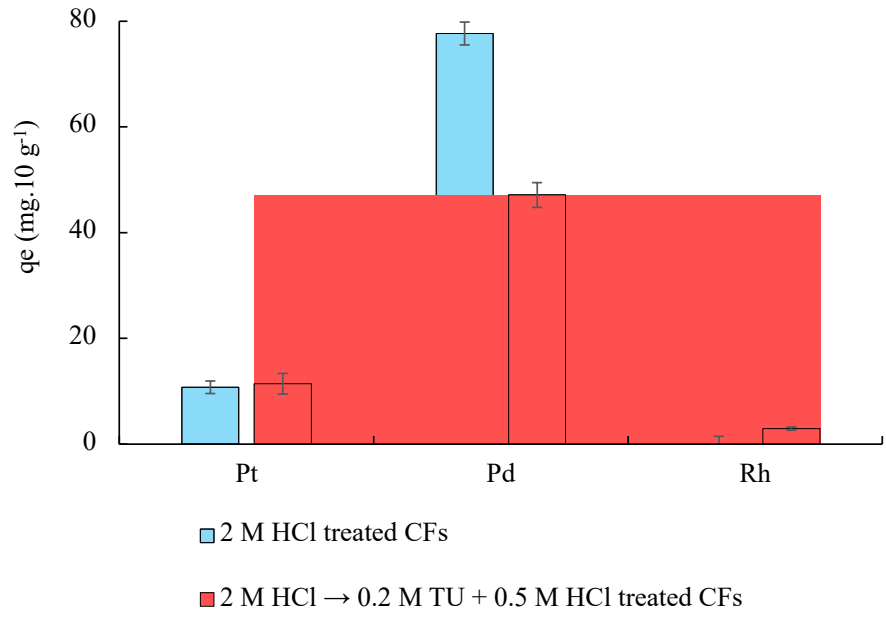

Figure S14. PGMs adsorption capacity of CFs exposed to 2 M HCl and also to 2 M HCl followed by 0.2 M TU + 0.5 M HCl from 1/6 MixC leachate. CF dosage of 10 $g.L^{-1}$, temperature at 303 K and a contact time of 360 min.

2.11. Thermogravimetric analysis

The thermal decomposition behavior of CF before and after Pd adsorption was investigated using thermogravimetric analysis (TGA) to evaluate the thermal stability of the materials. Figure S15 presents the TGA curves of raw CF and CF containing Pd. A minor weight loss below 150 °C was attributed to the evaporation of free and bound water (Sharma et al., 2017). Both samples remained thermally stable up to 200 °C. Beyond this point, a significant weight loss was observed between 240 and 400 °C (Figure S15), corresponding to the degradation of protein molecules. This includes helix denaturation, skeletal degradation, and the destruction of peptide bridge chain linkages (Sharma et al., 2017). According to the literature, this process involves the breakdown of disulfide bonds, resulting in the release of sulfur dioxide and hydrogen sulfide (Idris et al., 2014; Sharma et al., 2017; Wang et al., 2016). After pyrolysis, the residual weights were 90% for raw CF and 87% for CF with adsorbed Pd. The slightly higher residual mass for Pd–adsorbed CFs suggests that Pd might have enhanced the carbonization process, likely through a catalytic effect (Shetty and Hegde, 2024).

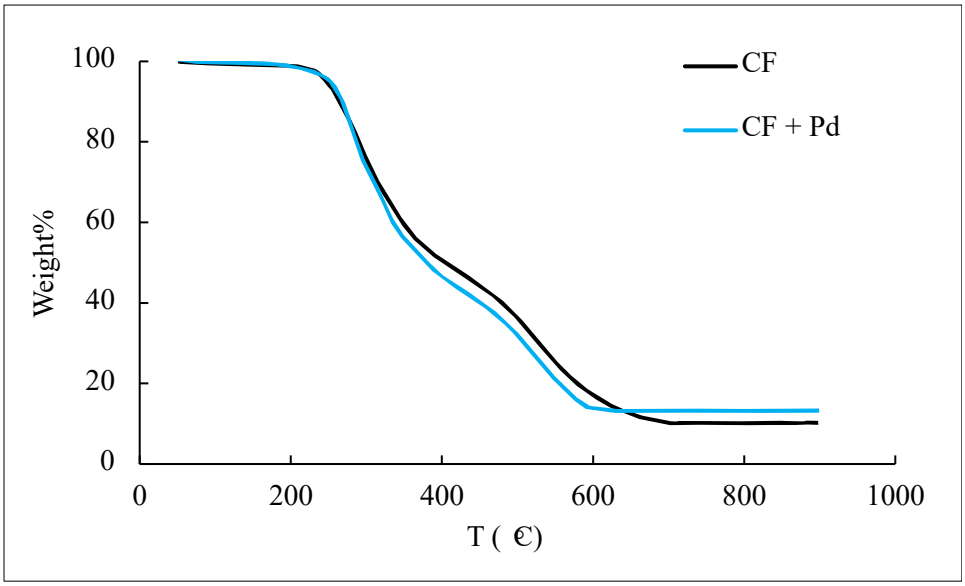

Figure S15. Thermogravimetric analysis (TGA) curves of raw CFs and Pd–adsorbed feathers (CF + Pd), showing weight loss (%) as a function of temperature (°C). (CFs obtained from adsorption studies in optimized conditions, and contain 14.82 ± 0.32, 4.70 ± 0.25 and 2.07 ± 0.08 $mg.g^{-1}$ of Pd, Pt and Rh).

3. References

Abd–Elhamid, A.I., Abu Elgoud, E.M., Aly, H.F., 2023. Adsorption of palladium from chloride aqueous solution using silica alginate nanomaterial. Int. J. Biol. Macromol. 253, 126754. https://doi.org/10.1016/j.ijbiomac.2023.126754

Akioka, S., Hirai, S., Ise, T., Gando, N., Alharbi, M.A.H., 2021. Selective recovery of palladium by wool resin and woven wool fabric resinrbents. Hydrometallurgy 203, 105629. https://doi.org/10.1016/j.hydromet.2021.105629

Ammi Said, A., Amara, M., Kerdjoudj, H., 2013. The effect of thiourea as a complexing agent on the separation of metallic ions through cation exchange membranes by Donnan dialysis. Ionics 19, 177–183. https://doi.org/10.1007/s11581–012–0724–x

Awadalla, F.T., Molnar, R.E., Ritcey, G.M., 1990. Recovery of platinum group metals (pgm) from acidic solutions by reduction precipitation with sodium borohydride. CA2016492A1.

Chatterjee, A., Abraham, J., 2019. Desorption of heavy metals from metal loaded sorbents and e–wastes: A review. Biotechnol. Lett. 41, 319–333. https://doi.org/10.1007/s10529–019–02650–0

Goc, K., Benke, G., Kluczka, J., Pianowska, K., Malarz, J., Leszczyńska–Sejda, K., 2024a. Application of ion–exchange dynamic conditions in the recovery of precious metals from refining waste. Sci. Rep. 14, 15026. https://doi.org/10.1038/s41598–024–66086–x

Goc, K., Kluczka, J., Benke, G., Malarz, J., Pianowska, K., Leszczyńska–Sejda, K., 2024b. Precipitation of Precious Metals Concentrates from Post–Elution Solutions from Ion–Exchange Processes. Minerals 14, 625. https://doi.org/10.3390/min14060625

Godlewska–Żyłkiewicz, B., Sawicka, S., Karpińska, J., 2019. Removal of Platinum and Palladium from Wastewater by Means of Biosorption on Fungi Aspergillus sp. and Yeast Saccharomyces sp. Water 11, 1522. https://doi.org/10.3390/w11071522

Hubicki, Zbigniew, Wołowicz, A., 2009. A comparative study of chelating and cationic ion exchange resins for the removal of palladium(II) complexes from acidic chloride media. J. Hazard. Mater. 164, 1414–1419. https://doi.org/10.1016/j.jhazmat.2008.09.053

Hubicki, Z., Wołowicz, A., 2009. Adsorption of palladium(II) from chloride solutions on Amberlyst A 29 and Amberlyst A 21 resins. Hydrometallurgy 96, 159–165. https://doi.org/10.1016/j.hydromet.2008.10.002

Hubicki, Z., Wołowicz, A., Wawrzkiewicz, M., 2009. Application of commercially available anion exchange resins for preconcentration of palladium(II) complexes from chloride–nitrate solutions. Chem. Eng. J. 150, 96–103. https://doi.org/10.1016/j.cej.2008.12.007

Idris, A., Vijayaraghavan, R., Rana, U.A., Patti, A.F., MacFarlane, D.R., 2014. Dissolution and regeneration of wool keratin in ionic liquids. Green Chem 16, 2857–2864. https://doi.org/10.1039/C4GC00213J

Mishra, V., 2014. Biosorption of zinc ion: a deep comprehension. Appl. Water Sci. 4, 311–332. https://doi.org/10.1007/s13201–013–0150–x

Sari, A., Mendil, D., Tuzen, M., Soylak, M., 2009. Biosorption of palladium(II) from aqueous solution by moss (Racomitrium lanuginosum) biomass: Equilibrium, kinetic and thermodynamic studies. J. Hazard. Mater. 162, 874–879. https://doi.org/10.1016/j.jhazmat.2008.05.112

Sharma, S., Gupta, A., Chik, S.M.S.T., Kee, C.G., Mistry, B.M., Kim, D.H., Sharma, G., 2017. Characterization of keratin microparticles from feather biomass with potent antioxidant and anticancer activities. Int. J. Biol. Macromol. 104, 189–196. https://doi.org/10.1016/j.ijbiomac.2017.06.015

Shetty, A., Hegde, G., 2024. Synthesis and characterization of biowaste–derived porous carbon supported palladium: a systematic study as a heterogeneous catalyst for the reduction of nitroarenes. React. Kinet. Mech. Catal. 137, 2989–3004. https://doi.org/10.1007/s11144–024–02690–2

Škerget, M., Čolnik, M., Zemljič, L.F., Gradišnik, L., Semren, T.Ž., Lovaković, B.T., Maver, U., 2023. Efficient and Green Isolation of Keratin from Poultry Feathers by Subcritical Water. Polymers 15, 2658. https://doi.org/10.3390/polym15122658

Tran, H.N., 2022. Improper Estimation of Thermodynamic Parameters in Adsorption Studies with Distribution Coefficient K_D (q_e/C_e) or Freundlich Constant (K_F): Considerations from the Derivation of Dimensionless Thermodynamic Equilibrium Constant and Suggestions. Adsorpt. Sci. Technol. 2022. https://doi.org/10.1155/2022/5553212

Wang, K., Li, R., Ma, J.H., Jian, Y.K., Che, J.N., 2016. Extracting keratin from wool by using L–cysteine. Green Chem. 18, 476–481. https://doi.org/10.1039/C5GC01254F

Wang, Z., Kang, S., Won, S., 2021. Recovery of Pd(II) from Aqueous Solution by Polyethylenimine–Crosslinked Chitin Biosorbent. Coatings 11, 593. https://doi.org/10.3390/coatings11050593

Wojnicki, M., Socha, R.P., Pędzich, Z., Mech, K., Tokarski, T., Fitzner, K., 2018. Palladium(II) Chloride Complex Ion Recovery from Aqueous Solutions Using Adsorption on Activated Carbon. J. Chem. Eng. Data 63, 702–711. https://doi.org/10.1021/acs.jced.7b00885

Wołowicz, A., Hubicki, Z., 2012. Ion Exchange Recovery of Palladium(II) from Acidic Solutions Using Monodisperse Lewatit SR–7. Ind. Eng. Chem. Res. 51, 16688–16696. https://doi.org/10.1021/ie302304c

Won, S.W., Yun, Y.–S., 2013. Recovery of metallic palladium from hydrochloric acid solutions by a combined method of adsorption and incineration. Chem. Eng. J. 218, 303–308. https://doi.org/10.1016/j.cej.2012.12.052

Zhang, L., Li, B., Shao, P., Zhou, X., Li, D., Hu, Z., Dong, H., Yang, L., Shi, H., Luo, X., 2023. Selective capture of palladium from acid wastewater by thiazole–modified activated carbon: Performance and mechanism. Environ. Res. 238, 117253. https://doi.org/10.1016/j.envres.2023.117253

Zhou, L., Liu, J., Liu, Z., 2009. Adsorption of platinum(IV) and palladium(II) from aqueous solution by thiourea–modified chitosan microspheres. J. Hazard. Mater. 172, 439–446. https://doi.org/10.1016/j.jhazmat.2009.07.030